Received: 7 October 2025 | Revised: 27 May 2026 | Accepted: 27 May 2026

DOI: 10.1111/joa.70193

Journal of Anatomy | ANATOMICAL SOCIETY WILEY

ORIGINAL ARTICLE

Anatomical description of the jaw muscles and theoretical bite force assessment in South American opossums using manual and digital dissection methods

Alice Melekian[1] | Vincent Decuypere[1] | Anthony Herrel[2,3,4,5] | François Clarac[1] | Sandrine Ladevèze[1]

[1]Centre de Recherche en Paléontologie Paris (CR2P), Muséum National d'Histoire Naturelle, CNRS, Sorbonne Université, Paris, France

[2]Mécanismes Adaptatifs et Evolution, UMR 7179, Muséum National d'Histoire Naturelle, CNRS, Paris, France

[3]Department of Biology, Evolutionary Morphology of Vertebrates, Ghent University, Ghent, Belgium

[4]Functional Morphology Laboratory, Department of Biology, University of Antwerp, Antwerp, Belgium

[5]Naturhistorisches Museum Bern, Bern, Switzerland

Correspondence
Alice Melekian, Centre de Recherche en Paléontologie Paris (CR2P), Muséum National d'Histoire Naturelle, CNRS, Sorbonne Université, Paris, France.
Email: alice.melekian@gmail.com; alice.melekian@mnhn.fr

Funding information
Centre de Recherche en Paléontologie Paris; Muséum National d'Histoire Naturelle, Grant/Award Number: ATM-AGRIP; European Synchrotron Radiation Facility, Grant/Award Number: ESFR Experiment LS-2427 ED19/2015

Abstract

Marsupials (Marsupialia, Mammalia) represent an ecologically diverse clade. This is particularly true for opossums (South American marsupials), which are, however, often difficult to observe and collect. Consequently, few studies have focused on their bite force and the muscles of their masticatory apparatus, and only scant information on the diet of many species exists. Here we describe the masticatory muscles of several previously unstudied opossum species including *Caenolestes fuliginosus*, *Dromiciops gliroides* and *Monodelphis touan*. We calculate the bite force of these species using data from both manual and digital dissections and compare their theoretical bite forces with literature data. Additionally, we explore the differences between manual and digital dissection to determine the muscle PCSA (physiological cross-sectional area). The results highlighted variation in the position of the muscular attachments and muscle size as well as in the distribution of each muscle in the *masticatory apparatus*, with a larger temporal complex in *M. touan* and a larger zygomasseteric complex in *D. gliroides*. The bite forces are coherent with estimates from the literature suggesting that our biomechanical model is reliable. The comparison between manual and digital dissections showed that while digital dissection allows an overall description of the masticatory muscles, it is more complex to accurately describe the different subdivisions of the muscle bundles. The use of digital volumes to calculate the PCSA remains to be evaluated. Digital dissection data can complement manual dissection data, provided that the composite structure of muscles and the physiological changes during impregnation with contrast agents are better understood.

KEYWORDS
contrast-enhanced CT-scan, dissection, Marsupialia, masticatory musculature, skull myology

François Clarac and Sandrine Ladevèze co-last authors. The authors have participated equally in the design and the supervision of this study.

1 | INTRODUCTION

Marsupials (Marsupialia, Mammalia) are one of the three major clades of extant mammals, alongside monotremes (Monotremata) and placentals (Placentalia). Defined as the least inclusive clade containing *Didelphis marsupialis* Linnaeus, 1758, *Caenolestes fuliginosus* (Tomes, 1863) and *Phalanger orientalis* (Pallas, 1766) (Beck et al., 2014). Marsupialia comprises over 400 species (Eldridge et al., 2019; Mammal Diversity Database, 2025) that are distributed across seven clades occurring in the Americas and Oceania. Marsupials exhibit a remarkable ecological diversity including arboreal (e.g. *Marmosa murina*), fossorial (e.g. *Notoryctes typhlops*), semi-aquatic (e.g. *Chironectes minimus*), gliding (e.g. *Petaurus breviceps*) and terrestrial (e.g. *Dasyurus viverrinus*) lifestyles. Their diets are equally diverse, encompassing carnivory (e.g. *Sarcophilus harrisii*), insectivory (e.g. *Myrmecobius fasciata*), herbivory (e.g. *Macropus rufus*) and opportunistic omnivory (e.g. *Didelphis virginiana*). However, the ecological and functional traits of many marsupials, particularly South American species, remain understudied.

Biting is a key functional trait allowing dietary diversification in different mammalian clades (e.g. Aguirre et al., 2003; Cornette et al., 2015; Ginot et al., 2018; Kraus et al., 2022; Santana et al., 2012). In mammals, mastication involves several muscles—including the temporal, the pterygoid, the masseter, the zygomaticomandibular and the digastric muscles whose activation patterns vary during jaw opening and closing (Gorniak, 1985; Thexton & Hiiemae, 1975). The elements of the masticatory apparatus form a morphological module, meaning that they are more functionally integrated with each other than with other body regions (Eble, 2005; Ziermann et al., 2021). The masticatory modules differ between marsupials and placentals and are associated with skeletal modules such as the neurocranium, which includes the squamosal, posterior cranial bones, mandible and vertebrae (Ziermann et al., 2021). Morphological changes in masticatory muscles often influence skeletal structures and vice versa (Cornette et al., 2013; Fabre et al., 2018; Ferreira-Cardoso et al., 2020). Diet and feeding strategies are known to be critical drivers of the cranial and mandibular morphology as well as the masticatory muscle architecture (Bubadué et al., 2023; Kienle et al., 2022). For example, the dietary hardness influences the masticatory muscle efficiency (Santana et al., 2010, 2012), while other adaptations, such as echolocation, also impact craniofacial structures (Giacomini et al., 2022; Jacobs et al., 2014; Takeuchi et al., 2024). Phylogeny plays an additional role, as distantly related species with similar ecological roles often exhibit divergent morphological adaptations to similar functional demands (Fabre et al., 2018; Ferreira-Cardoso et al., 2020). Moreover, development further constraints these adaptations, particularly due to the early onset of suckling behavior in marsupials (Fabre et al., 2021). Additionally, head size (Abreu & Astúa, 2025) and social behavior associated with sexual selection and territoriality also influence the bite force (Naretto et al., 2014; Thomas et al., 2015). In vivo studies have shown that bite force is to some degree plastic and variable over lifetime in response to both diet changes (Anderson et al., 2014) and behavioral choices (Santana & Dumont, 2009). However, recent studies have shown that natural selection acts on variation in bite force (Herrel et al., 2016) and that bite force is heritable (Zablocki-Thomas et al., 2021).

Despite the global interest that has been given to the study of bite force in mammals, marsupials remain understudied in this context. This gap reflects a broader taxonomic bias in biological research, where marsupials are often sidelined or studied only for comparative purposes with placentals. Consequently, detailed descriptions of marsupial masticatory muscles remain fewer in number, as compared to those concerning placentals (but see Coues, 1872; Turnbull, 1970; Minkoff et al., 1979; Warburton, 2009; Thomas et al., 2024; Decuypere et al., 2025; Abreu & Astúa, 2025). Moreover, variations in the muscle nomenclature further complicate comparisons across studies, with marsupial diversity being frequently excluded from nomenclatural standardisation efforts (Diogo et al., 2016; Druzinsky et al., 2011).

This study aims to start filling these gaps by examining the masticatory muscle anatomy across a several species of opossums (i.e. South American marsupials). Here we provide new anatomical descriptions and bite force estimates for underrepresented species, particularly two South American marsupials: the monito del monte opossum (*Dromiciops gliroides*) and the shrew opossum (*C. fuliginosus*), for which myological data remain scarce. This work integrates digital dissections with contrast-enhanced CT-scanning to perform 3D-reconstruction of soft tissues and modeling of bite force to reduce reliance on destructive manual dissection, extending its applicability to rare species (i.e. rare in natural history collections and with understudied ecologies). As part of this effort, we further compare manual and digital dissection techniques using two model opossum species, *M. murina* and *Monodelphis touan*, to preliminary assess the consistency and reliability of digital methods.

2 | MATERIALS AND METHODS

2.1 | Sample

This study focuses primarily on small opossums, whose bite force and masticatory muscles remain poorly studied and largely undescribed. Our primary opossum model is *M. murina*, two individuals of which were manually dissected in a previous study (Decuypere et al., 2025) and then scanned through X-ray microtomography, with contrast staining beforehand (see below).

Marmosa murina (M1496, adult female, collected in 2014) and *M. touan* (M2838, adult male, collected in 2017) were collected in the field during expeditions in French Guiana and are part of the JAGUARS ('Joindre l'Amazonie et la Guyane: Animaux, Ressources et Sciences », Institut Pasteur of French Guiana, https://kwata.net/) collection. To complement this dataset and expand knowledge on the anatomy of rare South American taxa, two specimens with available synchrotron data (Ladevèze et al., ESFR Experiment LS-2427 ED19/2015) were included: *C. fuliginosus* (MNHN.CG.1982.940, adult male) and *D. gliroides* (MNHN.CG.1981.1075, adult male). All

specimens were preserved in a 70° aqueous ethanol solution and listed in Table 1.

The specimens were initially scanned using micro-computed tomography (micro-CT) at the AST-RX platform (UAR 2AD) of the MNHN, utilising a 'v|tome|x L240-180' (Baker Hughes Digital Solutions). A first scan was performed to capture bone morphology. Afterward, the specimens underwent a chemical treatment (see Section 2.3.1. Manual dissection method) to enhance the density and visibility of muscular tissues. They were then re-scanned using CT imaging. Additionally, two ethanol-preserved specimens from the collections of the MNHN (*C. fuliginosus* and *D. gliroides*) were scanned at the Synchrotron (ESRF Grenoble) as part of a previous project.

2.2 | Nomenclature and discrimination

All muscles involved in bite force production in marsupials were identified (e.g. the masseter, zygomaticomandibularis, temporalis and the medial and lateral pterygoid muscles).

Four main criteria are used in order to discriminate the muscle bundles and fascicules:

- *The presence of an aponeurosis* which has lighter grayscale than the muscles in digital dissection and is identifiable by a white layer separating muscles when performing manual dissection.
- *The compactness/texture and orientation* of the bundles as fibres of a muscular unit are more similar within one unit than between units.
- *The presence of interstitial space* between muscle fascicules and bundles. This space shows a darker grayscale than muscles in digital dissection and allows the tweezers to pass through during manual dissection.
- *Comparative anatomy* using the literature. The location of its *origin* and *insertion*, the innervation by the branches of the *masseteric nerve*.

The nomenclature used for all the specimens follows both Turnbull (1970) and the standardised *Nomina Veterinaria* (5th edition; Waibl et al., 2012). We also describe *M. murina* according to the nomenclature used in Decuypere et al. (2025) as the specimen that we here digitally dissected was manually dissected in this previous study.

The digastric muscle, only involved in jaw opening, was excluded from the bite force calculations and will not be illustrated as the muscles are removed during the manual dissection. However, it is described for *M. touan* as it was observed in manual dissection.

2.3 | Dissections

2.3.1 | Manual dissection

Manual dissection was performed on one side of the specimen. All masticatory muscles, along with digastric muscles, the tongue and eye tissue, were removed from the dissected side. The skull and muscles from the non-dissected side were immersed in a 5% phosphomolybdic acid (PMA) solution diluted in 70% ethanol during 3 to 9 weeks, depending on the impregnation time required for muscle staining. PMA was selected as a contrast agent because it allows clear differentiation between skeletal muscles and surrounding soft tissues. Its high atomic number gives a clearer contrast enhancement (Descamps et al., 2014; Pauwels et al., 2013) than iodine-based contrast agents, which is a key property for the study of small specimens. Although phosphomolybdic acid is known to diffuse more slowly than iodine-based contrast agents (Pauwels et al., 2013), this limitation was not restrictive in the present study due to the small size of the specimens.

Dissected muscles were stored in 70% ethanol before being weighed. Weights were obtained considering the whole mass of muscle—tendinous and muscular part—using a METTLER AE 100 balance after blotting the muscles dry to remove the excess ethanol. The volume of muscles was estimated using both the muscle mass and its density for comparison with the digital dissection and the calculation of the PCSA.

Individual muscles were submerged in a 30% aqueous nitric acid solution for 48 h to dissolve connective tissues, following the method of Loeb and Gans (1986). After connective tissues were dissolved, the nitric acid was removed and replaced by a 50% aqueous solution of glycerol. Fibres were isolated using tweezers and photographed under a Leica WILD M3Z binocular microscope with oblique lighting (Intralux® 4000, Geprüfte Sicherheit) on a black background. The images were analysed in ImageJ (Schneider et al., 2012) and the fibre length is estimated by the mean length of 10 fibres (i.e. a standard number which is assumed to be representative as the muscles are small).

TABLE 1 Species, their inventory number, the sources of their dissection data, the scan resolution of their bone and the scan resolution of their soft tissues.

Species	Inventory number	Dissection data	Scan resolution (bone) (µm)	Scan resolution (soft tissues) (µm)
Caenolestes fuliginosus	MNHN.CG.1982.940	Virtual	6.23	6.23
Dromiciops gliroides	MNHN.CG.1981.1075	Virtual	6.23	6.23
Marmosa murina	M1496	Manual and virtual	14	14
Monodelphis touan	M2838	Manual and virtual	25	13.4

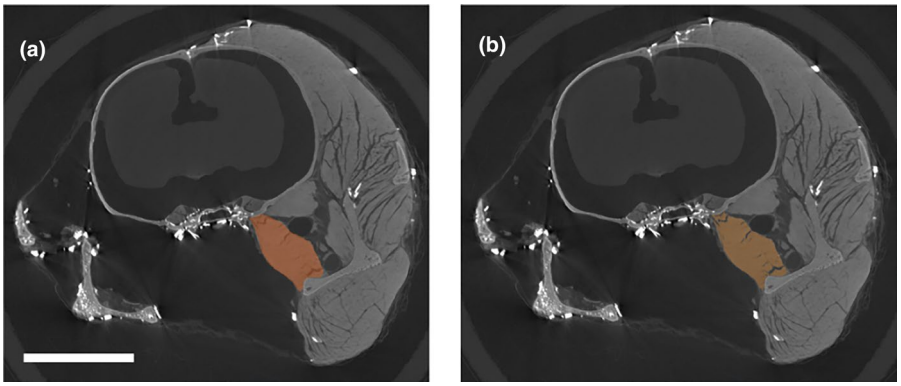

FIGURE 1 Coronal view of the half-dissected head of *Marmosa murina* (M1496). The two images show the differences, on the same slice, between a segmentation with the gaps (a) and without (b) for the *M. pterygoideus medialis*. Scale bar: 5 mm.

2.3.2 | Digital dissection

After soaking in PMA, specimens were re-scanned. Digital dissections were performed with Mimics 3D v.23.1 (Materialise, Leuven, Belgium). The muscles were segmented slice by slice because grayscale thresholds were insufficient to isolate them. Manual outlining was done every 5–10 slices using the Mimics' interpolation tool. The segmentation was simultaneously processed in sagittal, coronal and axial views, with a 3D rendering displayed in a separate window that allowed monitoring of the modelling progress.

Muscles were segmented individually and separated from the remaining cranial structures using Boolean operations. Each muscle was segmented based on its observed morphology during manual dissection.

3D objects were created from segmented masks and exported as .stl files for further treatment in Geomagic Wrap (3DSystems, Morrisville, NC). In order to manage the file size, the mesh density was reduced to about one million polygons per object while maintaining sufficient resolution for measurements.

Muscle volume and fibre lengths were estimated using Mimics' volume and distance measurement tools. The gaps between muscle fibres correspond to the extracellular matrix (ECM), composed of interstitial fluid and fibrous connective tissues, including the perimysium and endomysium (Purslow, 2002; Sleboda et al., 2020), which contain different collagen types (Light & Champion, 1984). Because specimens were stored in ethanol and impregnated by phosphomolybdic acid, tissue dehydration and shrinkage were expected to occur, particularly affecting extracellular compartments. These chemical treatments may therefore alter the apparent size of inter-fibre spaces, potentially leading to biases in digital volume estimation. To assess the influence of extracellular space representation on muscle volume estimates, two complementary segmentation strategies were applied. In the first strategy, the extracellular matrix was included in the muscle segmentation, yielding a maximal apparent muscle volume. In the second strategy, inter-fibre spaces corresponding to low-density voxels were excluded to obtain a minimal apparent muscle volume. The two resulting volume estimates (with and without extracellular matrix) are considered as upper and lower bounds of muscle volume estimates (Figure 1).

Exclusion of inter-fibre spaces was achieved by identifying an intensity threshold that captured the majority of low-density darker regions, corresponding to extracellular spaces. A Boolean minus operation was then applied to remove these voxels from the initial muscle mask. Segmentation results were visually inspected to avoid inadvertent removal of muscle fibres.

2.4 | Biomechanical model

2.4.1 | Muscle force estimation

Bite force estimation first relies on calculating the theoretical maximal force that is generated by each masticatory muscle:

$$FM_i(N) = PCSA\left(cm^2\right).FM_s\left(N.cm^{-2}\right)$$

The PCSA is the physiological cross section area of the muscle. FM_s is the muscle specific tension which have a constant value of 30 $N.cm^{-2}$ for mammals (Nigg & Herzog, 1994). PCSA was determined as:

$$PCSA\left(cm^2\right) = \frac{m_i(g)}{l_i(cm).\rho\left(g.cm^{-3}\right)}.cos\theta$$

where: m_i: muscle mass; l_i: fibre length of the muscle; ρ: muscle density which is a constant value of 1.056 $g.cm^{-3}$ (Leonard et al., 2020; Méndez & Keys, 1960).

The pennation angle was excluded, consistent with previous studies (Ginot et al., 2018; Hartstone-Rose et al., 2018) because it has been argued to be more accurate to calculate PCSA without pennation angle when the multipennate muscles are too complex as found in jaw muscles (Hartstone-Rose et al., 2018; Hartstone-Rose et al., 2019; Martin et al., 2020). Correction factors were applied to estimate in vivo muscle mass based on preservation methods: 1.32 for formalin and 1.69 for 70% ethanol (Leonard et al., 2022a, 2022b). As the PMA increases the density of the muscles in order to enhance

them, it also increases their volume. To date, and as far as we know, no correction factors are available in literature to correct this effect.

2.4.2 | Anatomical coordinate system (ACS) and bite force calculation

To project each muscle force onto the jaw-closing axis and calculate the theoretical bite force, an anatomical coordinate system was defined in Geomagic. The origin was set at the temporomandibular joint (TMJ) and the system is defined by three axes (i.e. the anteroposterior axis x, the mediolateral axis y and the dorsoventral axis z), which enable the vectorial projection of each muscle force.

Each masticatory muscle is modelled as a vector connecting the centroid of the insertion area (IA) on the mandible to the centroid of the origin area (OA) on the skull. Each vector is projected onto the three axes, allowing the calculation of each muscle force using:

$$FM_{(X,Y,Z)} = FM.cos\alpha_{(X,Y,Z)}$$

For the specimens whose muscles were segmented, the origin and insertion areas are defined by a Boolean intersection operation between the 3D model of the muscle and the 3D model of the skull or mandible. For the specimens that were manually dissected, the areas were manually traced based on muscle observations during dissections or available dissection data (i.e. Abreu & Astúa, 2025; Thomas et al., 2024). The centroid of these areas is then calculated using the 'centroid' tool in the 'feature' tab. Finally, the various lever arms are determined with the 'distance' tool in the 'analysis' tab, by measuring the orthogonal projection of the distance between the centroid of each muscle IA and the ACS origin along the X axis (as schematised in Figure 2).

Each muscle in the system generates an individual moment Miz ($N.cm^{-1}$) that reflects its ability to rotate the mandible around the jaw articulation (i.e. the origin of the ACS). This moment is the product of the vertical (z) component of the muscle force FM (in Newtons) and the lever arm d (in cm), which corresponds to the longitudinal distance (x) between the pivot point (TMJ) and the centroid of the muscle's insertion area (IA). Moments were calculated as:

$$M_{iz}\left(N.cm^{-1}\right) = FM_{iz} \times d_{(TMJ-cIA)x}$$

where FM_{iz} is the vertical component of the force, and $d_{(TMJ-cIA)x}$ is the lever arm length.

The theoretical bite force is calculated as the ratio between the sum of the moments $\sum M_{iz}$ of the masticatory muscles and the out-lever $d_{(TMJ-tooth)x}$, which corresponds to the longitudinal distance (x) between the pivot point (TMJ) and the tooth where the bite force is applied. To compute the bilateral bite force, this ratio is multiplied by two:

$$FM_t = \frac{\sum M_{iz}}{d_{(TMJ-tooth)x}} \times 2$$

The theoretical bite forces were compared to results from other modelling studies: Abreu and Astúa (2025) and Decuypere et al. (2025).

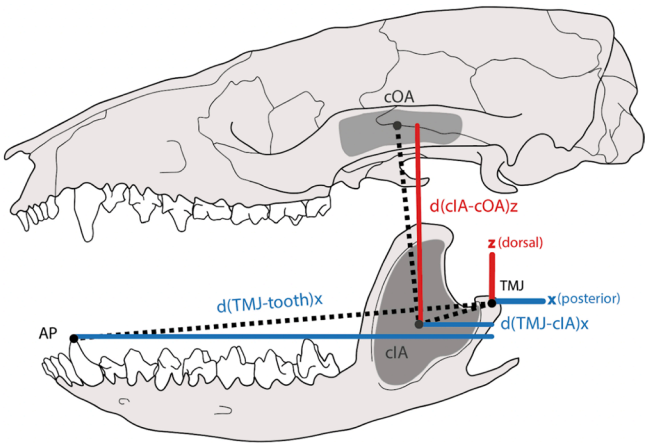

FIGURE 2 Figure showing the various distances used in the bite force calculation on the lateral view of the skull and mandible of *Monodelphis brevicaudata* (modified from Wible, 2003). cIA, Centroid of the insertion of the *M. zygomaticomandibularis*; cOA, Centroid of the origin of the *M. zygomaticomandibularis*; TMJ, Temporomandibular joint; x, Anteroposterior axis; z, Dorsoventral axis; Distances: Black, dashed line: Total distance between points. Red: Distance along the dorsoventral axis. Blue: Distance along the anteroposterior axis.

3 | RESULTS

3.1 | Manual and digital muscular descriptions

3.1.1 | Digastric muscle (Di)

The digastric muscle consists of two parts, anterior and posterior, connected by a thick tendon. A thin aponeurosis covers the anterior part and thickens towards the posterior part. The muscle originates from the most posterior part of the exoccipital and inserts medioventrally on the mandibular body, from the level of the third lower premolar (pm3) to the angular process. The anterior part is diamond-shaped, long and flat, while the posterior part is thicker and tapered. The tendon connecting the two parts is located medioventrally to the superficial masseter muscle. The muscle fibres are oriented anteroposteriorly throughout. This muscle is not digitally described as the beforehand manual dissection requires dissecting both the anterior and posterior parts in order to reach the pterygoids. It is also not accounted for in the masticatory apparatus as this muscle is only involved in the opening of the jaw (Gorniak, 1985).

3.1.2 | The Zygomasseteric complex (Figure 3; attachment areas in Figure A1)

The zygomasseteric complex constitutes from 32.05% (*C. fuliginosus*) to 44.31% (*D. gliroides*) of the masticatory apparatus. It is composed of two main muscle groups: the *M. masseter* and the *M. zygomaticomandibularis*. The masseter includes three *pars*

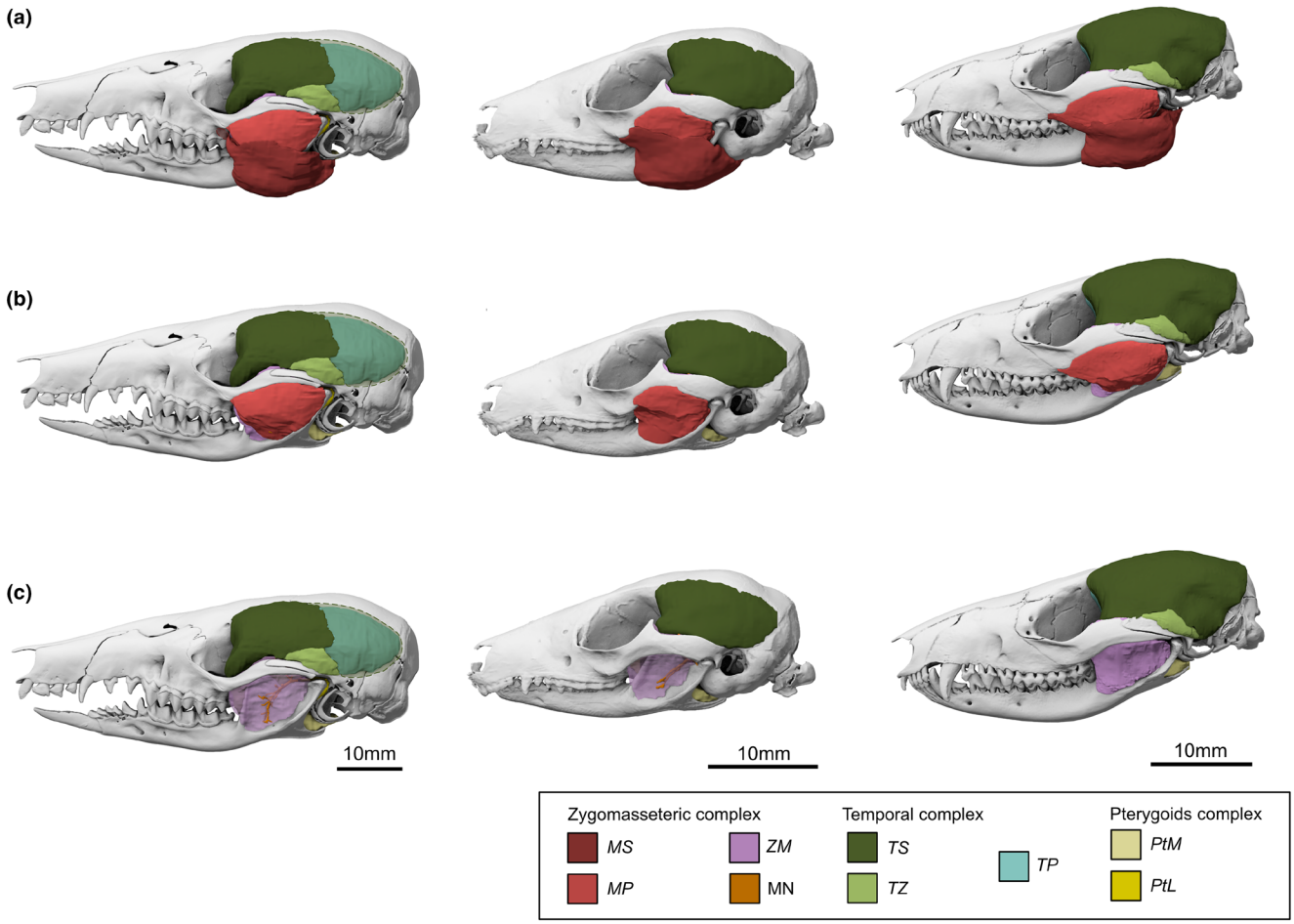

FIGURE 3 Comparison in lateral view of the zygomasseteric complex in *Caenolestes fuliginosus* (left), *Dromiciops gliroides* (middle) and *Monodelphis touan* (right). (a) All the muscles in-situ. (b) *Masseter superficialis* (*MS*) removed. (c) *Masseter profundus* (*MP*) removed, *zygomaticomandibularis* (*ZM*) and masseteric nerve (MN) visible.

for *M. murina* (i.e. *M. masseter pars superficialis*, *M. masseter pars intermedius*, *M. masseter pars profundus* as described in Decuypere et al., 2025) and two for the other species (*M. masseter pars superficialis* and *pars profundus*). The *M. masseter pars intermedius* described by Decuypere et al. (2025) for *M. murina* can be attributed here to *M. masseter pars superficialis* for its anterior part and *M. masseter pars profundus* for its posterior part, following the description and insertion areas of Turnbull (1970). In this regard, only the *M. masseter pars superficialis* and *M. masseter pars profundus* will be described here as we did not find the *M. masseter pars intermedius* either in *M. murina* during digital dissections (Figure 4) or in the other species of the present study (in agreement with Turnbull, 1970).

M. masseter pars superficialis (MS)

The superficial masseter muscle accounts for approximately 13.86% (*C. fuliginosus*) to 22.5% (*D. gliroides*) of the total masticatory muscle mass (see Figure 5 to compare all the muscles proportions). A thick aponeurosis clearly separates it from the digastric muscle and covers its entire surface. The muscle is thick and round, originating from a thick tendon located at the lateral posterior part of the maxilla, above the posterior section of the second upper molar M2 (*M. touan*, considering all the thick tendon) or the third upper molar M3 (*C. fuliginosus*, *D. gliroides*). It inserts ventrolaterally on the mandibular ramus along the masseteric fossa, from the posterior third lower molar m3 to the angular process and extends upward to the condylar process.

M. masseter pars profundus (MP)

The deep masseter muscle represents from approximately 6.76% to 10.98% of the total masticatory muscle mass. This pars was found as divided into a *pars intermedius* and a *pars profundus* in *M. murina* during the manual dissection although the *pars intermedius* was not visible in the digital dissection. The muscle is discriminated from the superficial portion by a thick aponeurosis that attaches on the mandible but does not extend up to the zygomatic arch, making the discrimination more difficult on the dorsal side.

It has a rounded and flat appearance, originating from the lower lateral ventral part of the zygomatic arch. The middle of the muscle extends over the lower half of the zygomatic arch for *D. gliroides*. The muscle inserts ventrally in the masseteric fossa, from its most posterior part to almost the third lower molar (m3) level. Its fibres are oriented towards the posterior part of the zygomatic arch.

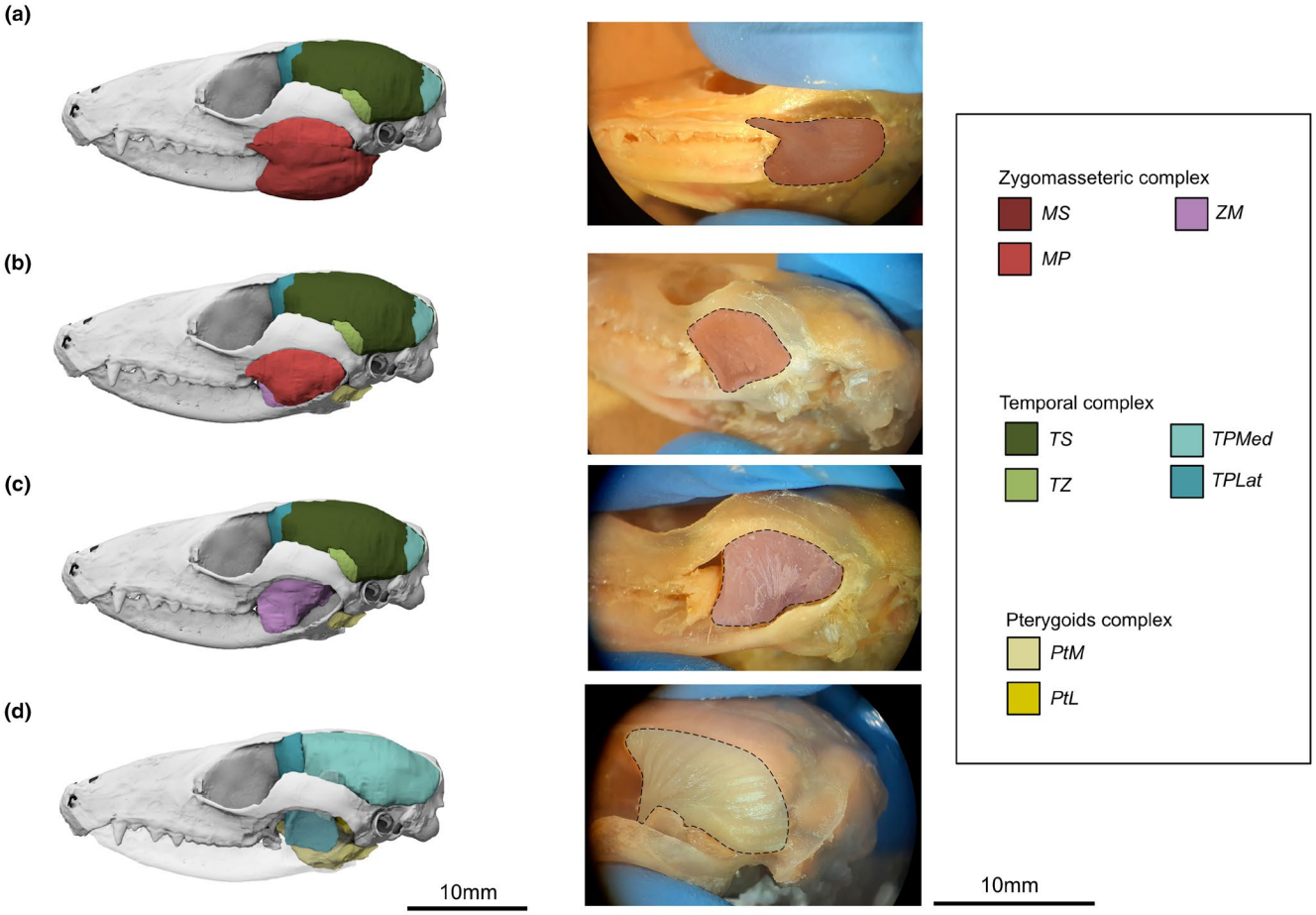

FIGURE 4 Comparison in lateral view of the temporal and pterygoid complexes in *Caenolestes fuliginosus* (left), *Dromiciops gliroides* (middle) and *Monodelphis touan* (right). (a) The two complexes. (b) Temporalis superficialis and suprazygomatica removed. (c) Only the pterygoid complex. (d) Focus on the temporalis profunfus.

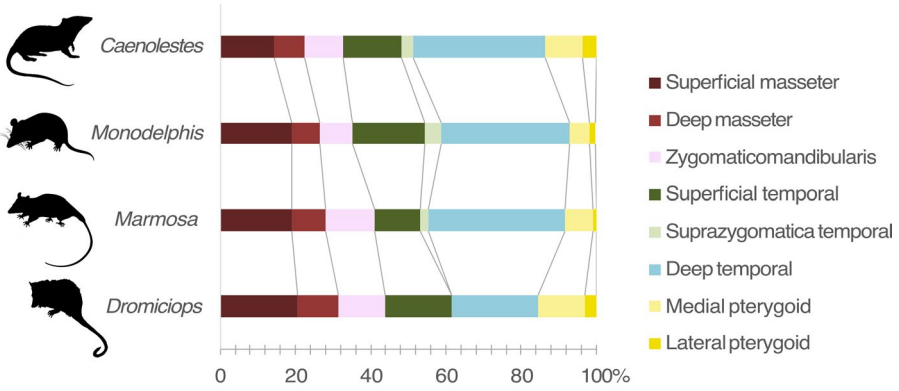

FIGURE 5 Percentage comparison of each muscle in the total volume (mm^3) of the masticatory apparatus for, from up to bottom, *Caenolestes fuliginosus*, *Monodelphis touan*) *Marmosa murina* and *Dromiciops gliroides*. Silhouettes by Sarah Werning, Milena Cavalcanti, Patricia Pilatti & Diego Astúa available on https://www.phylopic.org/.

M. zygomaticomandibularis (ZM)

The zygomaticomandibularis muscle represents from approximately 5.38% (*M. touan* in manual dissection) to 14.15% (*M. murina* in digital dissection) of the total masticatory muscle mass. The muscle is overestimated by the digital dissection method compared to the manual dissection. The entire muscle is crossed by a trunk of the masseteric nerve (MN) that goes through near its middle for *C. fuliginosus* (as also described in Turnbull, 1970) or more near its posterior part as found in *D. gliroides* (Figure 3c). The whole muscle originates from the medial facet of the zygomatic arch. It inserts laterally onto the masseteric fossa below the insertion of *M. temporalis pars suprazygomatica* and on the lower

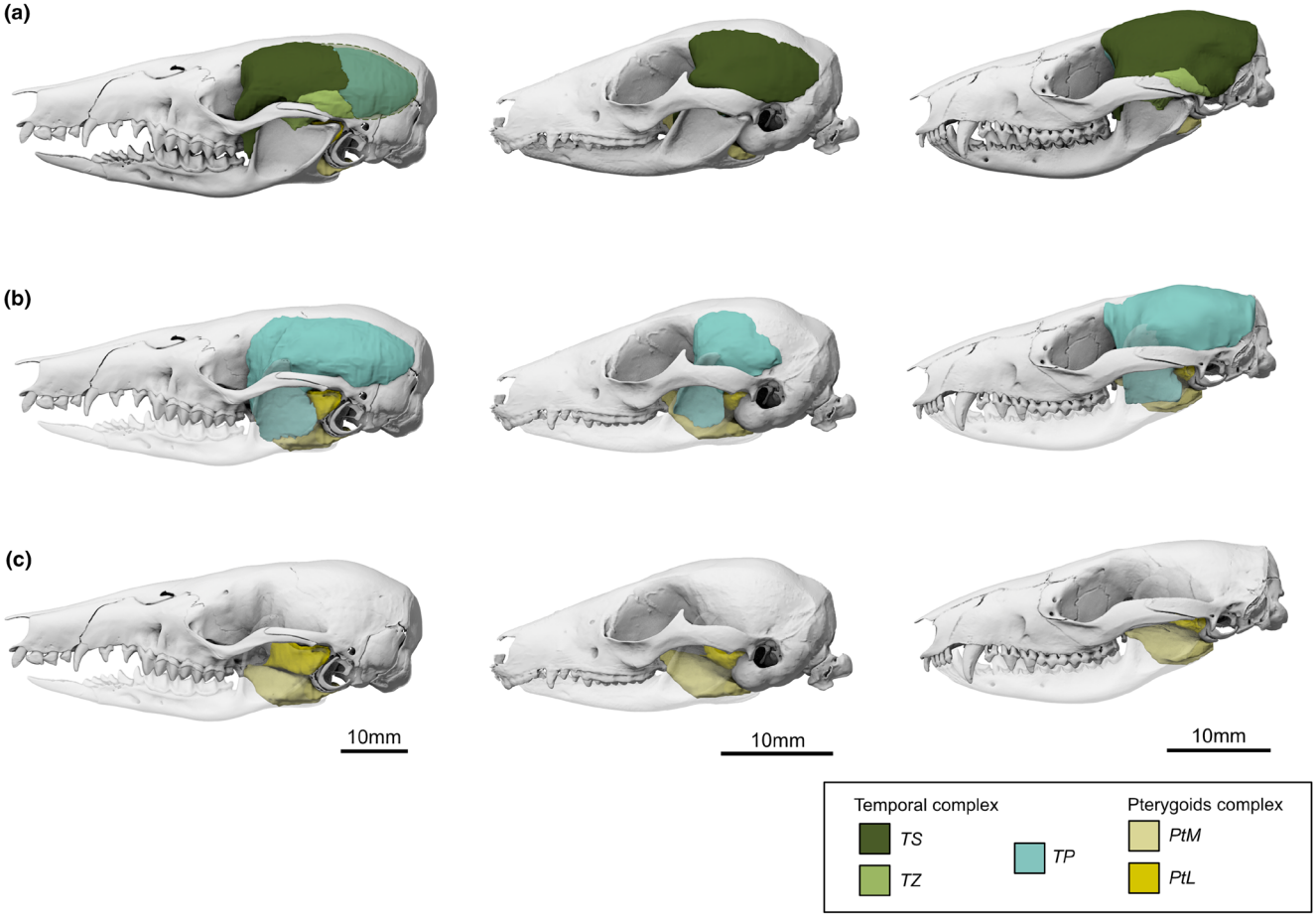

FIGURE 6 Comparison in lateral view of the temporal and pterygoid complexes in *Caenolestes fuliginosus* (left), *Dromiciops gliroides* (middle) and *Monodelphis touan* (right). (a) The two complexes in-situ. (b) Temporalis superficialis and suprazygomatica removed. (c) Pterygoid complex only.

half of the coronoid crest under the insertion of *M. temporalis superficialis*. Its fibres are oriented more dorsoventrally than the fibres of the *M. masseter pars profundus*, as described by Turnbull, 1970 (Figure A2).

The muscle is composed of two pars that can be separated with the direction of fibres during manual dissection of *M. touan* but cannot be separated during digital dissection (Figure A2).

The *anterior pars* originates along the anterior third medial edge of the zygomatic arch and inserts across the masseteric fossa, above the insertion of the deep masseter muscle. Its fibres are oriented in the direction of the jugal bony prominence. The *posterior pars* originates along the posterior two thirds medial edge of the zygomatic arch and inserts across the masseteric fossa, above the insertion of the deep masseter muscle. Its fibres are oriented in the direction of the squamosal.

3.1.3 | The temporal complex (Figure 6; attachment areas in Figure A1)

The temporal complex constitutes from 40.09% (*D. gliroides*) to 58.26% (*M. touan*, digital dissection) of the masticatory apparatus. It is composed of a suprazygomatic (*M. temporalis pars suprazygomatica*), a superficial (*M. temporalis pars superficialis*) and a deep *pars* (*M. temporalis pars profundus*).

M. temporalis pars suprazygomatica (TZ)

The *M. temporalis pars suprazygomatica* accounts for 2.22% (*M. murina*, digital dissection) to 6.07% (*M. touan*, manual dissection) of the total masticatory muscle mass. It is external to the superficial temporalis muscle. This *pars* was not found in the digital dissection of *D. gliroides* as the temporal complex does not extend upward of the zygomatic arch.

The muscle originates from the posterior part of the zygomatic arch, extending along half of its lateral and medial surface as a thin muscle layer. It inserts dorsolaterally onto the coronoid crest and extends to the posterior part of the coronoid process during manual dissection but this extension is not visible during digital dissection (see *M. touan* in Figures 6 and A2).

M. temporalis pars superficialis (TS)

The superficial temporalis muscle constitutes from 12.23% to 19.93% of the total masticatory muscle mass. It is covered by a thick aponeurosis that extends over the dorsolateral surface of the

zygomatic arch. The muscle is composed of two unequal layers: one round and fleshy upper layer (see TS1 in Figure A2) and one flatter and moon-shaped lower part (see TS2 in Figure A2). TS2 fibres are connected on the lateral (superficial) side of the aponeurosis *planum tendinum temporalis* described by Turnbull (1970). During digital dissection, TS1 is visible but dorsally merges with the *M. temporalis pars profundus* as the *planum tendinum temporalis* becomes thinner further away from the coronoid process. TS2 could not be identified digitally.

The whole *M. temporalis pars superficialis* is digitally either overestimated or underestimated compared to manual dissection, as the separation with the *M. temporalis pars profundus* remains difficult due to the absence of the *planum tendinum temporalis* on the dorsal and posterior part of the temporal complex (see in Figures 6 and 4 the absence or presence of the posterior part of TS depending on the tomographic slices). The muscle inserts dorsolaterally on the upper half of the coronoid process and originates along the sagittal and nuchal crests, bordering the frontal, parietal, interparietal and squamosal bones. The fibres are fan-shaped, directed towards the coronoid process.

M. temporalis pars profundus (TP)

The deep temporal muscle accounts for 22.20% (*D. gliroides*) to 36.40% (*C. fuliginosus*) of the total masticatory muscle mass. The entire *pars* origin extends over parietal, frontal, squamosal, interparietal, alisphenoid and palatine bones, reaching the palatine region of the interorbital fossa and is inserted into the medial surface of the coronoid process. It has two supplementary *pars* (the *M. temporalis pars profundus lateralis* TPLat and *M. temporalis pars profundus medialis* TPMed) that can be separated during dissection thanks to a change of fibre direction, which was partly observed during the digital dissection. However, the separation during digital dissection is difficult (see Figure 4) and remains uncertain as no other anatomical clues than fibre direction (e.g. aponeurosis or interstitial space) can be used. These pars are therefore only described from the manual dissection of *M. touan* (Figure A1).

The lateral part of the deep temporal muscle (*M. temporalis pars profundus lateralis*, TPLat) accounts for 4.29% of the total masticatory muscle mass. It is difficult to distinguish from the medial part of the deep temporal muscle due to the presence of abundant connective tissue. The TPLat originates from the posterior part of the supraorbital margin of the frontal bone, extending from the sagittal crest to the frontal-palatal suture. It inserts anteriorly on the medial and dorsal side of the coronoid process. Its fibres are more parallel and dorsoventrally directed than the *M. temporalis pars profundus medialis*.

The medial bundle of the deep temporalis muscle (*M. temporalis pars profundus medialis*, TPMed) is the most massive masticatory muscle, accounting for 31.58% of the total masticatory muscle mass. The fibres are on the medial (deep) side of the *planum tendinum temporalis*. It originates posteriorly from the lateral region of the frontal bone, covering parts of the parietal, alisphenoid and squamosal bones. It inserts medially on the coronoid process, posterior to the insertion of the TPLat. Its fibres are band-shaped in the direction of the insertion.

3.1.4 | The pterygoid complex (Figure 6)

The pterygoid complex constitutes from 6.5% (*M. touan*, manual dissection) to 15.6% (*D. gliroides*) of the masticatory apparatus and is composed of *M. pterygoideus medialis* and *M. pterygoideus lateralis*.

M. pterygoideus lateralis (PtL)

The lateral pterygoid muscle represents from 0.57% (*M. murina*, digital dissection) to 3.73% (*C. fuliginosus*, digital dissection) of the total masticatory muscle mass, making it the smallest masticatory muscle. It originates ventrolaterally on the alisphenoid and inserts on the medial border, near the mandibular condyle. Its fibres are parallel in the direction of the mandibular condyle.

M. pterygoideus medialis (ptm)

The medial pterygoid muscle constitutes from 6.20% (manual dissection of *M. touan*) to 12.41% (non-corrected digital dissection of *D. gliroides*) of the total masticatory muscle mass. It is long and flat, originating from the ventrolateral edge of the pterygoid and posterior part of the palatine. It inserts on the medial side of the mandibular ramus, filling a part (*Dromiciops*) or entirely (*Monodelphis*, *Caenolestes*) the pterygoid pit while extending over all the angular process. Its fibres are parallel in the direction of the anterior part of the pterygoid pit.

3.2 | Comparison of physiological parameters

The muscle volumes that were computed digitally reveal a positive linear relationship with the same muscle volumes that were obtained from manual dissection (Figure 7). Whether taking interstitial spaces into account or not in digital reconstructions, values increased consistently in agreement with manually measured volumes so the relationship follows a linear trend. The deviation from the line of identity (green line, $x = y$) was not erratic. Instead, the discrepancy between manual and digital measurements increased progressively with muscle size, as indicated by regression slopes greater than 1 ($a = 1.36$ when interstitial spaces were excluded; $a = 1.50$ when included). However, the magnitude of this increase was not homogeneous across muscles: while most data points shifted upward in a relatively consistent manner, some muscles exhibited a more pronounced divergence (e.g. *M. zygomaticomandibularis* being more divergent than *M. masseter pars superficialis*).

The relative differences between manual and digital measurements vary according to methodological treatment (with vs. without interstitial spaces) and species. The difference between the volume

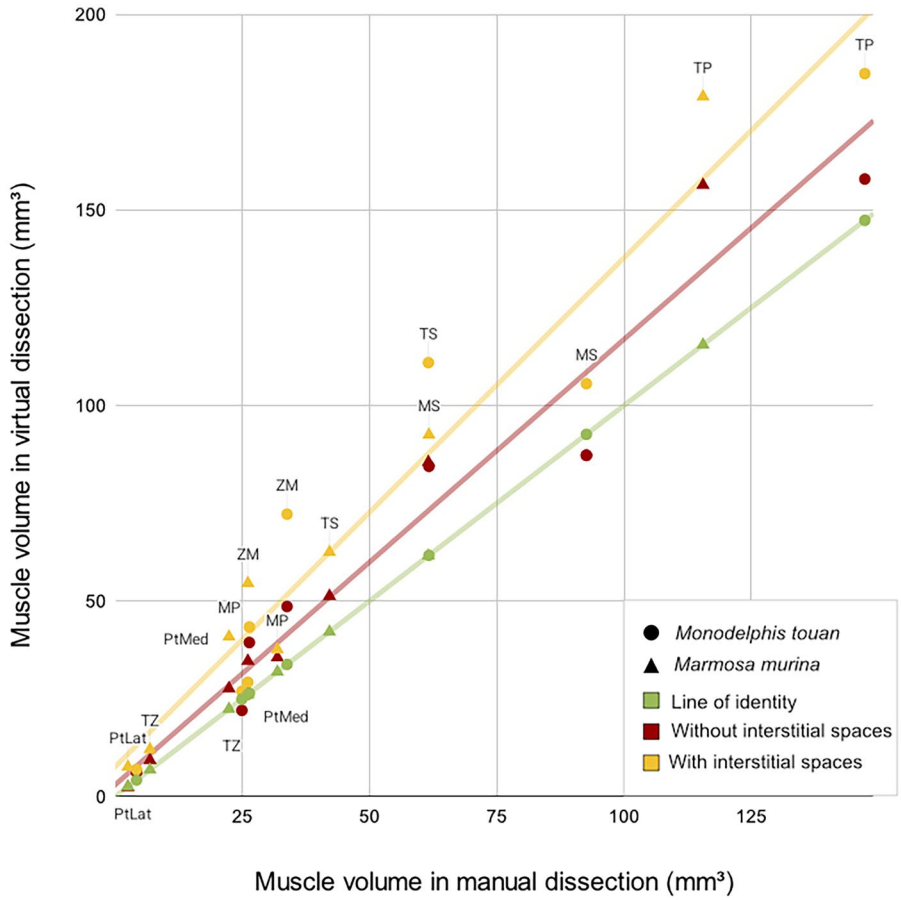

FIGURE 7 Comparison of ex-vivo (non-corrected) muscle volume between manual and virtual dissection (mm^3). Yellow: Volume with interstitial spaces; Red: Volume without interstitial spaces; Green: Line of identity $x = y$. *Marmosa murina* is represented by triangles and *Monodelphis touan* by circles.

ranges is under 70% while adding interstitial spaces and under 35% while excluding them (Supplementary data).

In both species, *M. murina* and *M. touan*, some muscles such as the *zygomaticomandibularis* and the *temporal* (excepting TZ) tend to show similar higher deviations, particularly when interstitial spaces are taken into account. Conversely, the pterygoid complex frequently exhibits lower deviations or values closer to zero (Figure 7).

The comparison of fibre lengths obtained using manual and digital dissection methods reveals a clear positive linear relationship between methodologies (Figure 8). The trend line exhibits a slope ($a = 0.843$) close to the line of identity (green line, $x = y$), indicating proportional scaling between methods. Overall, data points are tightly clustered around the trend line, demonstrating concordance between approaches.

Some muscles, however, show a greater deviation from the trend line, particularly the *M. zygomaticomandibularis*, *M. masseter pars profundus* and both the superficial and deep portions of the *M. temporalis*. The largest deviations from the trend line are observed in the species *M. murina*. Agreement between manual and digital methods remains particularly strong at lower fibre lengths (<3 mm), with only minor divergence. At higher fibre lengths (>5.5 mm), variability increases slightly, although the overall linear trend is maintained across the measurement range.

The relative differences between manual and digital fibre length measurements vary according to species (Figure 8). The difference between the methods ranges under 32% for *M. murina* and under 15% for *M. touan* (Supplementary data). The most impacted muscles are fan-shaped muscles, such as the superficial and deep parts of *M. masseter* or the superficial part of *M. temporalis*.

3.3 | Comparison of bite forces

The comparison between the bite forces estimated in this study and those reported in the literature shows that the digital dissection seems to estimate higher bite forces than manual dissection, as evidenced in the case of *M. murina* (M1496) (Table 2). For this specimen, the difference in the theoretical bite force that was calculated after both methods (i.e. manual and digital dissection) ranges between 1.18 and 4.11 Newtons. This difference increases when including the interstitial space in the 3D-models of the muscles (as it impacts the volume used for calculations). All bite forces increase as skull size increases.

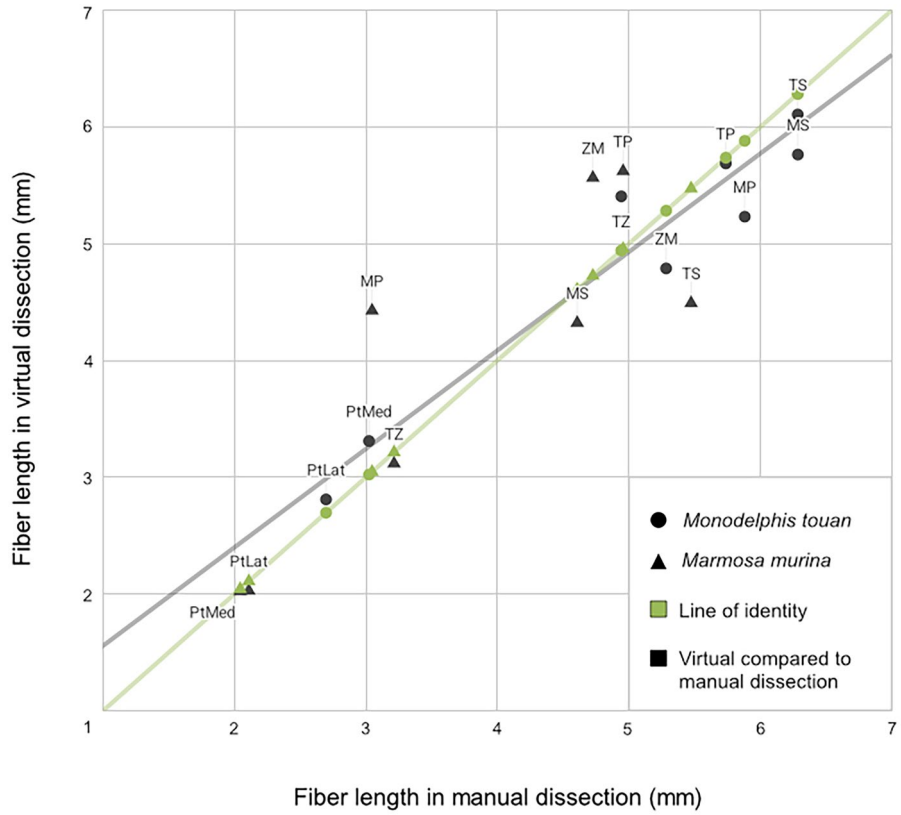

FIGURE 8 Comparison of muscle fibre lengths between manual and virtual dissection (mm). Black: Virtual fibre length depending on manual fibre length; Green: Line of identity $x = y$. *Marmosa murina* is represented by triangles and *Monodelphis touan* by circles.

TABLE 2 Comparison of minimal and maximal unilateral theoretical bite forces estimated in this study and in the literature.

	Marmosa murina, this study	*Marmosa murina*[a]	*Marmosa murina*[b]	*Monodelphis touan*	*Dromiciops gliroides*	*Caenolestes fuliginosus*
Skull size (cm)	3.51	3.51	3.624	3.22	2.96	6.11
Bite force at canine (N)	[5.99–7.53]	NA	4.126	[4.41–5.56]	[4.14–4.67]	[16.47–18.15]
Bite force at m1 (N)	[8.34–10.49]	NA	5.755	[7.46–9.44]	[5.86–6.49]	[22.69–25.012]
Bite force at m3 (N)	[11.42–14.35]	10.24	NA	[10.83–13.68]	[7.87–8.72]	[30.20–33.47]

Note: Skull sizes were measured from the tip of the nasal bone to the most posterior point of the nuchal crest.

[a]Based on data from Decuypere et al. (2025), M1496 specimen.

[b]Based on data from Abreu and Astúa (2025).

4 | DISCUSSION

4.1 | Variability of muscles in three orders of opossums

4.1.1 | Muscular proportions and attachment areas

This study highlights the existence of variability in the morphology of masticatory muscles among four species of extant opossums, particularly concerning attachment areas, fibre lengths, masses and contributions to total muscle mass. These findings, compared with previous studies (Turnbull, 1970; Ercoli et al., 2023; Decuypere et al., 2025), though based on a limited number of specimens, support the variability observed in Abreu and Astúa (2025). Furthermore, here we calculate the first theoretical bite force for three species and compare another one (*M. murina*) to published references (Decuypere et al., 2025). We describe the morphology of the masticatory muscles in some species that were not previously documented, such as *M. touan* (based on manual dissection data and digital dissection data), *D. gliroides* and *C. fuliginosus* (using only digital dissection data).

The preliminary data that we provide here already show variation in the position of the muscular attachments of the masticatory

muscles in opossums in agreement with Abreu and Astúa (2025). For example, the temporal attachments are less extensive in *Dromiciops gliroides* than in the two other species. These differences in the positioning of the attachment areas have an impact on the position of the centroid, on the resulting lever arm and therefore on the calculated bite force. In addition to the position of the attachment areas, muscles differ in their individual percentage of the total weight of the masticatory apparatus (Table 3). These interspecific differences could be related to different muscle involvement due for example to different diet constraints (as already suggested on a larger scale by Ercoli et al. (2023)). More specifically, we observe that species with omnivorous diets such as *M. murina* and *D. gliroides* (Lessa et al., 2023) appear to have a larger zygomasseteric complex, whereas species that share a predominant animal-based diet such as *M. touan* and *C. fuliginosus* (Lessa et al., 2023) have a larger temporal complex. Moreover, *M. murina* and *D. gliroides* also eat smaller items whereas *M. touan* and *C. fuliginosus* are capable of eating larger items such as rodents, snakes and scorpions (Lessa et al., 2023; Martin & González-Chávez, 2016). Such observations must nevertheless be confirmed with more species before making any general statements. The pterygoid complex in *D. gliroides* and *C. fuliginosus* is larger than in any didelphid, suggesting differences that could be due to their phylogenetic distance rather than selective pressures on feeding adaptations.

4.1.2 | Muscular nomenclature and discrimination among marsupials

It is important to point out that these descriptions followed a nomenclature mostly based on Turnbull (1970) that does not match that of other authors such as Abreu and Astúa (2025), explaining at least in part the differences found between these descriptions. In fact, no specific nomenclature has been clearly defined for marsupials, although an attempt of homogenisation was made by Druzinsky et al. (2011). This represents a major problem that complicates comparisons and should be remedied in the future. Also, some differences on the attachment areas between the zygomaticomandibularis and the temporal have been noticed between this study and Abreu and Astúa (2025) for the genus *Monodelphis*, highlighting the differences during the discrimination of principal bundles during manual dissection. These differences are also found between Decuypere et al. (2025) and Abreu and Astúa (2025) for the genus *Marmosa*. This could be explained by the fibrous texture and the difficulty to access the attachment areas of the *M. zygomaticomandibularis*. In this study, the discrimination of this muscle is based on different criteria such as the fibre direction, which is more dorsoventral than the M. *masseter pars profundus* (Turnbull, 1970) and more lateromedial than the *M. temporalis pars superficialis*. Depending on the scan resolution, it was also distinguished by the presence of the deep branches of the masseteric nerve that pass through the *M. zygomaticomandibularis* (e.g. the description of *D. marsupialis* by Turnbull (1970) and dogs by Tomo et al. (1993) and Yang et al. (2010)) with some of them reaching the *M. temporalis* (Yang et al., 2010). This work therefore highlights the importance of establishing a consistent nomenclature within marsupials, in order to compare the studies.

4.2 | Advantages and limitations of the digital dissection

4.2.1 | Main limitations of the digital dissection

The use of digital methods as a replacement for manual dissections is a growing topic of interest (Ginot & Blanke, 2024; Katzke et al., 2022). Replacing manual dissection (a destructive method which removes muscles) with digital dissection (a fully non-destructive method based on synchrotron scanning) would help preserve rare or historical specimens by also allowing their descriptions. These new descriptions must be interpreted cautiously. Digital dissections are less precise as the connective tissue does not allow one to distinguish the muscles the same way as in the manual dissection. In fact, these tissues make the fibres form a distinct muscle unit by being attached to each other. Also, only the thicker parts of aponeuroses are visible during digital dissection; separation is more complicated in areas where it is not visible, as it was shown with the *planum tendinum* in the temporal. As a matter of fact, in the digital dissection of *M. murina*, the fascicles of the temporal could not be separated as they were in the manual dissection (Decuypere et al., 2025), and in the other species digitally dissected here, the separation between the superficial and deep temporal was difficult. Moreover, the *zygomaticomandibularis* is also complicated to segment as it is less compact than other muscles. Additionally, tendons may not always be accounted for during digital dissection. This was the case for the tendon connecting the superficial masseter to its origin in *M. murina*, which was not visible during digital dissection, reducing the attachment area of the muscle's origin and impacting the centroid position of its origin area.

4.2.2 | Main advantages of the digital dissection

Digital dissection, therefore, requires prior knowledge of muscle and skeletal anatomy for greater accuracy. However, it allows certain structures that are less visible during manual dissection to be seen, such as the trigeminal nerve and its ramifications. It also allows a better three-dimensional visualisation of the muscle architecture and attachment areas, which are more precise for certain muscles such as the medial and lateral pterygoid that are more difficult to observe during manual dissection. For the specimens that were scanned using absorption contrast X-ray (Synchrotron light), it is possible to visualise the soft tissues and the endocranial features, without any destruction. On the contrary, in stained specimens, some alterations occur (Hedrick et al., 2018; Moayedi et al., 2025), but all the soft

TABLE 3 Percentage comparison of each muscle in the total volume (mm^3) of the masticatory apparatus for different species, different methodologies and with literature.

		Virtual dissection	Manual dissection (Decuypere et al., 2025)	Manual dissection (Abreu & Astúa, 2025)	Manual dissection	Virtual dissection	Manual dissection (Turnbull, 1970)	Virtual dissection	Virtual dissection
Masseter superficialis	*MS*[a]	[18.14–20.13]%	19.38%	25.90%	22.55%	[18.97–19.15]%	15%	[20.23–21.06]%	[13.86–14.72]%
Masseter profundus	*MP*[a]	[8.5–9.39]%	8.63%	4.80	7.77%	[6.76–7.82]%	9.80%	[10.98–10.88]%	[8.14–7.92]%
Zygomaticomandibularis	*ZM*	[14.15–11.58]%	11.79%	3.40%	5.38%	[9.80–7.62]%	9.40%	[13.08–11.60]%	[10.05–10.59]%
Zygomasseteric complex		**[40.79–41.10]%**	**39.74%**	**34.10%**	**35.70%**	**[35.53–34.58]%**	**34.20%**	**[44.31–43.54]%**	**[32.05–33.23]%**
Temporalis superficialis	*TS*	[12.25–12.23]%	15.14%	38.20%	14.99%	[19.93–18.76]%	20.80%	[17.88–17.41]%	[16.66–14.49]%
Temporalis suprazygomatica	*TZ*	[2.37–2.22]%	2.28%		6.07%	[4.83–4.84]%			[3.04–3.12]%
Temporalis profundus lateralis	*TPLat*	[15.27–14.87]%	11.75%	21.50%	4.29%	[33.21–34.66]%	36.20%	[22.20–23.62]%	[33.57–36.40]%
Temporalis profundus medialis	*TPMed*	[19.82–22.42]%	21.76%		31.58%				
Temporal complex		**[49.71–51.74]%**	**50.93%**	**59.70%**	**56.93%**	**[57.97–58.26]%**	**57%**	**[40.09–41.03]%**	**[53.06–54.01]%**
Pterygoideus medialis	*PtMed*	[8.01–6.59]%	7.69%	6.20%	6.35%	[5.25–5.81]%	7.30%	[12.41–12.34]%	[10.88–9.11]%
Pterygoideus lateralis	*PtLat*	[1.49–0.57]%	0.89%	*NA*	1.03%	[1.25–1.35]%	1.60%	[3.18–3.09]%	[3.73–3.65]%
Pterygoids complex		**[9.50–7.16]%**	**8.58%**	**6.20%**	**7.38%**	**[6.5–7.16]%**	**8.90%**	**[15.6–15.43]%**	**[14.69–12.76]%**

Note: In bold, the addition of all the muscle (in percent) of one complex.

[a]*Masseter intermedius* from Decuypere et al. (2025) could not be found during the virtual dissection so the portion of the pars anterior was attributed to the *Masseter superficialis* and the portion of the pars posterior was attributed to the *Masseter profundus*, following both Turnbull (1970) and Decuypere et al. (2025) descriptions.

tissues stay in place. The main advantage of the digital dissection is both its repeatability and correctability when mistakes are made. When properly segmented with anatomical verification through manual dissection, 3D objects also have the potential to become educational tools for understanding muscle anatomy. Ultimately, these two methodologies are complementary and should be used together as much as possible in order to achieve the highest level of accuracy.

4.2.3 | Comparing physiological parameters

During this study, digital methods were essential for estimating volume and fibre length, parameters that are commonly used to calculate the theoretical bite force.

Nevertheless, muscle volume remains a topic of debate since some studies report similar volumes between manual and digital dissections (Katzke et al., 2022), while others find significant differences depending on the method that was used (Broyde et al., 2021; Ginot & Blanke, 2024). In our study, the variation between methodologies remained under 70% while adding interstitial spaces and under 35% while excluding these. The inclusion of interstitial spaces appears to affect muscles depending on their size and compactness. For example, muscles such as the *zygomaticomandibularis* and the *temporalis* consistently gave greater volume differences when interstitial spaces are included. This can be explained by the *zygomaticomandibularis* being much less compact than other muscles, as well as by the size of the *temporalis* muscle, which greatly increases the difference. Eliminating gaps is challenging due to the texture variation in the masticatory muscles. Indeed, within one same muscle, the texture may vary significantly, with less compact areas showing visible gaps between fibres and compact areas where gaps were harder to identify. Between distinct muscles, the structure difference (more or less spaces between the fibres) was even more pronounced, such as between the compact *superficial masseter* and the less compact *zygomaticomandibularis*. This texture variation likely affected the calculated volumes. Even though the minimal apparent muscle volume appears to be closer to the value that was calculated after manual dissection, excluding interstitial spaces also has limitations. Indeed, muscle is a composite structure that cannot be reduced to a binary model including only fibres and interstitial space (Spyrou et al., 2019). In order to fully understand the function of the full unit, it would be important to consider all components including collagen and interstitial fluid. To predict volume data for specimens that cannot be manually dissected, it would be valuable to create an inclusive model that would consider muscle tissue components beyond fibres. We here propose a very first step to this approach by showing a linear tendency observed between data that were extracted after both manual and digital dissections.

Additionally, the structural difference between distinct muscles might indicate differences in muscle density. If density differences are confirmed, PCSA calculations based on manual dissection data should also account for these differences by applying different muscle density.

For the fibre length the error ranged between 32% for *M. murina* and under 15% for *M. touan*. These differences can be explained by the fact that two different operators were involved in acquiring the *M. murina* data, whereas the *M. touan* data were acquired by one operator only. Since the fibre lengths studied are very small (few millimeters), the relative differences are quickly significant, but have a negligible impact on the resulting bite force when we compare the same specimens. The deviation from manual dissection seems to be related to the muscle size but also to its architecture. In fact, the biggest deviations are found in muscles with oblique or fan-shaped fibre arrangements such as the *masseter*, the *zygomaticomandibularis* and the superficial *temporal*. In contrast, muscles such as the pterygoids, which show smaller deviations and values closer to zero, possess a more parallel-fibred organisation. In this study, fibre length was simply estimated from direct measurements on CT-scan images (conventional micro-CT or Synchrotron). However, digital fibre lengths can be more precisely estimated, with minimal error (Ginot & Blanke, 2024; Katzke et al., 2022) using various techniques, such as importing and processing landmarks in R, using software like Amira (ThermoFisher Scientific) or ImageXd, the technique proposed by Püffel et al. (2021) or the R package *GoodFibes* (Arbour, 2023). In the future, it may be worthwhile to use one of these methods to validate the data obtained in this study.

Finally, all error margins were calculated for only two species and a single individual per species, so they do not reflect intraspecific variation. These are preliminary results that require more specimens in order to obtain more accurate estimations.

4.3 | Comparison of bite forces

The sample that we studied also showed a wide range of bite forces from the smallest specimen (*D. gliroides*) to the largest (*C. fuliginosus*). As previously suggested, marsupial bite force could be related to diet (although this has been refuted at the scale of Didelphidae by Abreu & Astúa, 2025, but remains to be tested using in vivo data) or the size of the species, which is also related to diet (Amador & Giannini, 2021; Brum et al., 2023; Silva-Neto et al., 2024). In fact, these two factors could be confounding. So far, our study cannot answer this debate, as our sample is too small so the effect of evolutionary allometry could not be tested. However, comparing data from this study to those from Abreu and Astúa (2025) seems to show the dependence between bite force and body size. This effect remains to be studied at a larger scale among different omnivorous marsupials to further estimate the impact of the phylogeny, size and diet respectively. However, it is important to note that the opossum diets can change depending on the season, and that much information is still lacking. The bite forces that we have calculated are consistent with previous bite force estimates based on biomechanical models (Decuypere et al., 2025 and Abreu & Astúa, 2025 to a lesser degree), suggesting that the biomechanical model we have used can be considered as reliable.

Nonetheless, it is important to note that our theoretical force calculations do not match the in vivo value in *M. murina* (Decuypere et al., 2025) and are based on two biomechanical constants (density and specific tension) that have so far only been calculated on a small sample of domesticated placentals (Leonard et al., 2020; Méndez & Keys, 1960; Nigg & Herzog, 1994). As a matter of fact, jaw opening is quite different between placentals and marsupials, with a greater jaw opening potential for the latter (Attard et al., 2011; Wroe et al., 2013), suggesting a different muscular extension ability. Such differences could introduce variability among values that have so far been considered constant when calculating the theoretical force. These constants should therefore be recalculated after more in vivo data in future work to further ensure the accuracy of the theoretical model.

ACKNOWLEDGEMENTS

We are thankful to Benoît de Thoisy (Institut Pasteur de Guyane and KWATA association) and Anne-Claire Fabre (Institute of Ecology & Evolution, Universität Bern, Switzerland) for the collection and the use of *Marmosa murina* (M1496) and *Monodelphis touan* (M2838) specimens. We also wish to thank M. Bellato, the operator of AST-RX (UAR DoHNEE, MNHN), for the CT acquisitions as well as N. Poulet and F. Goussard from the 3D platforms of the CR2P for their valuable insights on segmentation and all their helpful suggestions. SL warmly thanks Vincent Fernandez (beam ED19, ESRF, Grenoble) for his expertise and precious help during her stay at the European Synchrotron Radiation Facility. Our gratitude is extended to Diego Astúa and Juann A. F. H. Abreu (Laboratorio de Mastozoologia, Universidade Federal de Pernambuco, Brazil) for sharing their data and contributing to productive discussions. Finally, we would like to thank the reviewers of this article for their pertinent comments, which have significantly enhanced its quality. Open access publication funding provided by COUPERIN CY26.

FUNDING INFORMATION

This work forms part of A.M.'s MSc thesis in the 'Systématique Evolution Paléontologie' program at the Muséum National d'Histoire Naturelle à Paris (MNHN) and Sorbonne Université (SU). It was funded by an MSc fellowship from the Centre de Recherche en Paléontologie Paris (CR2P). The synchrotron scanning of *Caenolestes fuliginosus* and *Dromiciops gliroides* was funded by the ESFR Experiment LS-2427 ED19/2015. The field mission in French Guiana in 2017 was funded by an ATM-AGRIP grant from the MNHN awarded to A.-C. Fabre.

DATA AVAILABILITY STATEMENT

Data are now available at https://doi.org/10.48579/PRO/M0L57C (Marmosa murina), https://doi.org/10.48579/PRO/68FJMF (Caenolestes fuliginosus), https://doi.org/10.48579/PRO/IMIQHC (Dromiciops gliroides).

ORCID

Alice Melekian https://orcid.org/0009-0008-3065-436X
Vincent Decuypere https://orcid.org/0000-0002-4038-8877
Anthony Herrel https://orcid.org/0000-0003-0991-4434
François Clarac https://orcid.org/0000-0001-8247-8507
Sandrine Ladevèze https://orcid.org/0000-0001-6009-4107

REFERENCES

Abreu, J.A. & Astúa, D. (2025) Comparative and functional anatomy of masticatory muscles and bite force in opossums (Didelphimorphia, Didelphidae). The Anatomical Record.

Aguirre, L.F., Herrel, A., Van Damme, R. & Mathyssen, E. (2003) The implications of food hardness for diet in bats. *Functional Ecology*, 17, 201–212.

Amador, L.I. & Giannini, N.P. (2021) Evolution of diet in extant marsupials: emergent patterns from a broad phylogenetic perspective. *Mammal Review*, 51(2), 178–192.

Anderson, P.S., Renaud, S. & Rayfield, E.J. (2014) Adaptive plasticity in the mouse mandible. *BMC Evolutionary Biology*, 14, 1–9.

Arbour, J. (2023) GoodFibes: an R package for the detection of muscle fibers from diceCT scans. *Integrative Organismal Biology*, 5(1), obad030.

Attard, M.R., Chamoli, U., Ferrara, T.L., Rogers, T.L. & Wroe, S. (2011) Skull mechanics and implications for feeding behaviour in a large marsupial carnivore guild: the thylacine, Tasmanian devil and spotted-tailed quoll. *Journal of Zoology*, 285(4), 292–300.

Beck, R.M.D., Travouillon, K.J., Aplin, K.P., Godthelp, H. & Archer, M. (2014) The osteology and systematics of the enigmatic Australian oligo-Miocene metatherian *Yalkaparidon* (Yalkaparidontidae; Yalkaparidontia; Australidelphia; Marsupialia). *Journal of Mammalian Evolution*, 21(2), 127–172.

Broyde, S., Dempsey, M., Wang, L., Cox, P.G., Fagan, M. & Bates, K.T. (2021) Evolutionary biomechanics: hard tissues and soft evidence? *Proceedings of the Royal Society B: Biological Sciences*, 288(1945). Available from: https://doi.org/10.1098/rspb.2020.2809

Brum, M.N., Cáceres, N.C. & Bubadué, J.M. (2023) Evolutionary rates, disparity, and ecomorphology of the mandible in American marsupials. *Journal of Mammalian Evolution*, 30(1), 33–46.

Bubadué, J., Cáceres, N.C., Brum, M.N. & Meloro, C. (2023) Skull morphological evolution in faunivorous marsupials. In: *American and Australasian marsupials: an evolutionary, biogeographical, and ecological approach*. Cham: Springer International Publishing, pp. 431–451.

Cornette, R., Baylac, M., Souter, T. & Herrel, A. (2013) Does shape covariation between the skull and the mandible have functional consequences? A 3D approach for a 3D problem. *Journal of Anatomy*, 223(4), 329–336.

Cornette, R., Tresset, A., Houssin, C., Pascal, M. & Herrel, A. (2015) Does bite force provide a competitive advantage in shrews? The case of the greater white-toothed shrew. *Biological Journal of the Linnean Society*, 114, 795–807.

Coues, E. (1872) *On the osteology and myology of Didelphys virginiana*. Boston: Boston Society of Natural History.

Decuypere, V., Herrel, A., Grimal, Q., Germain, D., Fabre, A.C. & Ladevèze, S. (2025) Modelling marsupial mastication: the biomechanical bite model of the Linnaeus's mouse opossum *Marmosa murina* (Marsupialia, Didelphidae). *Journal of Anatomy*, 247(6), 1187–1203.

Descamps, E., Sochacka, A., De Kegel, B., Van Loo, D., Van Hoorebeke, L. & Adriaens, D. (2014) Soft tissue discrimination with contrast agents using micro-CT scanning. *Belgian Journal of Zoology*, 144(1).

Diogo, R., Bello-Hellegouarch, G., Kohlsdorf, T., Esteve-Altava, B. & Molnar, J.L. (2016) Comparative myology and evolution of marsupials and other vertebrates, with notes on complexity, Bauplan, and "scala naturae". *The Anatomical Record*, 299(9), 1224–1255.

Druzinsky, R.E., Doherty, A.H. & De Vree, F.L. (2011) Mammalian masticatory muscles: homology, nomenclature, and diversification. *Integrative and Comparative Biology*, 51(2), 224–234.

Eble, G.J. (2005) Morphological modularity and macroevolution: conceptual and empirical aspects.

Eldridge, M.D., Beck, R.M., Croft, D.A., Travouillon, K.J. & Fox, B.J. (2019) An emerging consensus in the evolution, phylogeny, and systematics of marsupials and their fossil relatives (Metatheria). *Journal of Mammalogy*, 100(3), 802–837.

Ercoli, M.D., Álvarez, A., Warburton, N.M., Janis, C.M., Potapova, E.G., Herring, S.W. et al. (2023) Myology of the masticatory apparatus of herbivorous mammals and a novel classification for a better understanding of herbivore diversity. *Zoological Journal of the Linnean Society*, 198(4), 1106–1155.

Fabre, A.C., Dowling, C., Portela Miguez, R., Fernandez, V., Noirault, E. & Goswami, A. (2021) Functional constraints during development limit jaw shape evolution in marsupials. *Proceedings of the Royal Society B*, 288(1949), 20210319.

Fabre, A.C., Perry, J.M., Hartstone-Rose, A., Lowie, A., Boens, A. & Dumont, M. (2018) Do muscles constrain skull shape evolution in Strepsirrhines? *The Anatomical Record*, 301(2), 291–310.

Ferreira-Cardoso, S., Fabre, P.H., de Thoisy, B., Delsuc, F. & Hautier, L. (2020) Comparative masticatory myology in anteaters and its implications for interpreting morphological convergence in myrmecophagous placentals. *PeerJ*, 8, e9690.

Giacomini, G., Herrel, A., Chaverri, G., Brown, R.P., Russo, D., Scaravelli, D. et al. (2022) Functional correlates of skull shape in Chiroptera: feeding and echolocation adaptations. *Integrative Zoology*, 17, 430–442.

Ginot, S. & Blanke, A. (2024) A comparison of dissection and 3D approaches to estimate muscle physiological cross-sectional area, validated by in vivo bite forces. *Journal of Experimental Biology*, 227(2), jeb246341.

Ginot, S., Herrel, A., Claude, J. & Hautier, L. (2018) Skull size and biomechanics are good estimators of in vivo bite force in murid rodents. *The Anatomical Record*, 301(2), 256–266.

Gorniak, G.C. (1985) Trends in the actions of mammalian masticatory muscles. *American Zoologist*, 25(2), 331–338.

Hartstone-Rose, A., Deutsch, A.R., Leischner, C.L. & Pastor, F. (2018) Dietary correlates of primate masticatory muscle fiber architecture. *The Anatomical Record*, 301(2), 311–324.

Hartstone-Rose, A., Hertzig, I. & Dickinson, E. (2019) Bite force and masticatory muscle architecture adaptations in the dietarily diverse Musteloidea (Carnivora). *The Anatomical Record*, 302, 2287–2299. Available from: https://doi.org/10.1002/ar.24233

Hedrick, B.P., Yohe, L., Vander Linden, A., Dávalos, L.M., Sears, K., Sadier, A. et al. (2018) Assessing soft-tissue shrinkage estimates in museum specimens imaged with diffusible iodine-based contrast-enhanced computed tomography (diceCT). *Microscopy and Microanalysis*, 24(3), 284–291.

Herrel, A., Lopez-Darias, M., Vanhooydonck, B., Cornette, R., Kohlsdorf, T. & Brandt, R. (2016) Do adult phenotypes reflect selection on juvenile performance? A comparative study on performance and morphology in lizards. *Integrative and Comparative Biology*, 56, 469–478.

Jacobs, D.S., Bastian, A. & Bam, L. (2014) The influence of feeding on the evolution of sensory signals: a comparative test of an evolutionary trade-off between masticatory and sensory functions of skulls in southern African horseshoe bats (Rhinolophidae). *Journal of Evolutionary Biology*, 27(12), 2829–2840.

Katzke, J., Puchenkov, P., Stark, H. & Economo, E.P. (2022) A roadmap to reconstructing muscle architecture from CT data. *Integrative Organismal Biology*, 4(1), obac001.

Kienle, S.S., Cuthbertson, R.D. & Reidenberg, J.S. (2022) Comparative examination of pinniped craniofacial musculature and its role in aquatic feeding. *Journal of Anatomy*, 240(2), 226–252.

Kraus, A., Lövy, M., Mikula, O., Okrouhlík, J., Bennett, N.C., Herrel, A. et al. (2022) Bite force in strictly subterranean rodent family, African mole-rats (Bathyergidae): the role of digging mode, social organisation, and ecology. *Functional Ecology*, 36, 2344–2355.

Leonard, K.C., Worden, N., Boettcher, M.L., Dickinson, E. & Hartstone-Rose, A. (2022a) Effects of freezing and short-term fixation on muscle mass, volume, and density. *The Anatomical Record*, 305(1), 199–208.

Leonard, K.C., Worden, N., Boettcher, M.L., Dickinson, E. & Hartstone-Rose, A. (2022b) Effects of long-term ethanol storage on muscle architecture. *The Anatomical Record*, 305(1), 184–198.

Leonard, K.C., Worden, N., Boettcher, M.L., Dickinson, E., Omstead, K.M., Burrows, A.M. et al. (2020) Anatomical and ontogenetic influences on muscle density. *Scientific Reports*, 11(1), 2114.

Lessa, L.G., Carvalho, R.F. & Astúa, D. (2023) Food habits of American marsupials. In: *American and Australasian marsupials: an evolutionary, biogeographical, and ecological approach*. Cham: Springer International Publishing, pp. 1095–1122.

Light, N. & Champion, A.E. (1984) Characterization of muscle epimysium, perimysium and endomysium collagens. *Biochemical Journal*, 219(3), 1017–1026.

Loeb, G.E. & Gans, C. (1986) *Electromyography for experimentalists*. Chicago: University of Chicago press.

Mammal Diversity Database. (2025) Mammal diversity database (version 2.4) [Data set]. Zenodo. https://doi.org/10.5281/zenodo.17033774

Martin, G.M. & González-Chávez, B. (2016) Observations on the behavior of *Caenolestes fuliginosus* (tomes, 1863) (Marsupialia, Paucituberculata, Caenolestidae) in captivity. *Journal of Mammalogy*, 97(2), 568–575.

Martin, M.L., Travouillon, K.J., Fleming, P.A. & Warburton, N.M. (2020) Review of the methods used for calculating physiological cross-sectional area (PCSA) for ecological questions. *Journal of Morphology*, 281(7), 778–789.

Méndez, J. & Keys, A. (1960) Density and composition of mammalian muscle. *Metabolism*, 9, 184–188.

Minkoff, E.C., Mikkelsen, P., Cunningham, W.A. & Taylor, K.W. (1979) The facial musculature of the opossum (*Didelphis virginiana*). *Journal of Mammalogy*, 60(1), 46–57.

Moayedi, A., Karali, K., Boese, M., Zekonyte, J., Radulovic, J. & Blunn, G. (2025) Evaluating the impact of contrast agents on micro and nano mechanics of soft-to-hard tissue interface. *Scientific Reports*, 15(1), 28267.

Naretto, S., Cardozo, G., Blengini, C.S. & Chiaraviglio, M. (2014) Sexual selection and dynamics of jaw muscle in Tupinambis lizards. *Evolutionary Biology*, 41, 192–200.

Nigg, B.M. & Herzog, W. (1994) Biomechanics of the musculo-skeletal system.

Pauwels, E., Van Loo, D., Cornillie, P., Brabant, L. & Van Hoorebeke, L. (2013) An exploratory study of contrast agents for soft tissue visualization by means of high resolution X-ray computed tomography imaging. *Journal of Microscopy*, 250(1), 21–31.

Püffel, F., Pouget, A., Liu, X., Zuber, M., van de Kamp, T., Roces, F. et al. (2021) Morphological determinants of bite force capacity in insects: a biomechanical analysis of polymorphic leaf-cutter ants. *Journal of the Royal Society Interface*, 18(182), 20210424.

Purslow, P.P. (2002) The structure and functional significance of variations in the connective tissue within muscle. *Comparative Biochemistry and Physiology Part A: Molecular & Integrative Physiology*, 133(4), 947–966.

Santana, S.E. & Dumont, E.R. (2009) Connecting behaviour and performance: the evolution of biting behaviour and bite performance in bats. *Journal of Evolutionary Biology*, 22(11), 2131–2145.

Santana, S.E., Dumont, E.R. & Davis, J.L. (2010) Mechanics of bite force production and its relationship to diet in bats. *Functional Ecology*, 24(4), 776–784.

Santana, S.E., Grosse, I.R. & Dumont, E.R. (2012) Dietary hardness, loading behavior, and the evolution of skull form in bats. *Evolution*, 66(8), 2587–2598.

Schneider, C.A., Rasband, W.S. & Eliceiri, K.W. (2012) NIH image to ImageJ: 25 years of image analysis. *Nature Methods*, 9(7), 671–675.

Silva-Neto, F.D.C., Pavan, S.E. & Astúa, D. (2024) Evolution, divergence, and convergence in the mandibles of opossums (Didelphidae, Didelphimorphia). *Current Zoology*, 70(4), 488–504.

Sleboda, D.A., Stover, K.K. & Roberts, T.J. (2020) Diversity of extracellular matrix morphology in vertebrate skeletal muscle. *Journal of Morphology*, 281(2), 160–169.

Spyrou, L.A., Brisard, S. & Danas, K. (2019) Multiscale modeling of skeletal muscle tissues based on analytical and numerical homogenization. *Journal of the Mechanical Behavior of Biomedical Materials*, 92, 97–117.

Takeuchi, H., Matsuishi, T.F. & Hayakawa, T. (2024) A tradeoff evolution between acoustic fat bodies and skull muscles in toothed whales. *Gene*, 901, 148167.

Thexton, A.J. & Hiiemae, K.M. (1975) The twitch-contraction characteristics of opossum jaw musculature. *Archives of Oral Biology*, 20(11), 743–748.

Thomas, P., Pouydebat, E., Hardy, I., Aujard, F., Ross, C.F. & Herrel, A. (2015) Sexual dimorphism in bite force in the grey mouse lemur. *Journal of Zoology*, 296(2), 133–138.

Thomas, V.J., Shaw, J., Tay, N. & Warburton, N.M. (2024) Comparative three-dimensional jaw muscle anatomy of marsupial carnivores (*Dasyurus* spp.) and the termite-eating numbat (*Myrmecobius fasciatus*). *Journal of Morphology*, 285(3), e21684.

Tomo, S., Hirakawa, T., Nakajima, K., Tomo, I. & Kobayashi, S. (1993) Morphological classification of the masticatory muscles in dogs based on their innervation. *Annals of Anatomy*, 175(4), 373–380.

Turnbull, W.D. (1970) Mammalian masticatory apparatus. *Fieldiana Geology*, 18, 149–356.

Waibl, H., Gasse, H., Constantinescu, G.M., Hashimoto, Y. & Simoens, P. (2012) Nomina anatomica veterinaria.

Warburton, N.M. (2009) Comparative jaw muscle anatomy in kangaroos, wallabies, and rat-kangaroos (Marsupialia: Macropodoidea). *The Anatomical Record: Advances in Integrative Anatomy and Evolutionary Biology: Advances in Integrative Anatomy and Evolutionary Biology*, 292(6), 875–884.

Wible, J.R. (2003) On the cranial osteology of the short-tailed opossum *Monodelphis brevicaudata* (Didelphidae, Marsupialia). *Annals-Carnegie Museum Pittsburgh*, 72(3), 137–202.

Wroe, S., Chamoli, U., Parr, W.C., Clausen, P., Ridgely, R. & Witmer, L. (2013) Comparative biomechanical modeling of metatherian and placental saber-tooths: a different kind of bite for an extreme pouched predator. *PLoS One*, 8(6), e66888.

Yang, H.M., Hu, K.S., Song, W.C., Park, J.T., Kim, H.J., Koh, K.S. et al. (2010) Innervation patterns of the canine masticatory muscles in comparison to human. *The Anatomical Record: Advances in Integrative Anatomy and Evolutionary Biology*, 293(1), 117–125.

Zablocki-Thomas, P., Lailvaux, S., Aujard, F., Pouydebat, E. & Herrel, A. (2021) Maternal and genetic correlations between morphology and physical performance traits in a small captive primate, *Microcebus murinus*. *Biological Journal of the Linnean Society*, 134, 28–39.

Ziermann, J.M., Boughner, J.C., Esteve-Altava, B. & Diogo, R. (2021) Anatomical comparison across heads, fore-and hindlimbs in mammals using network models. *Journal of Anatomy*, 239(1), 12–31.

SUPPORTING INFORMATION

Additional supporting information can be found online in the Supporting Information section at the end of this article.

How to cite this article: Melekian, A., Decuypere, V., Herrel, A., Clarac, F. & Ladevèze, S. (2026) Anatomical description of the jaw muscles and theoretical bite force assessment in South American opossums using manual and digital dissection methods. *Journal of Anatomy*, 00, 1–19. Available from: https://doi.org/10.1111/joa.70193

APPENDIX

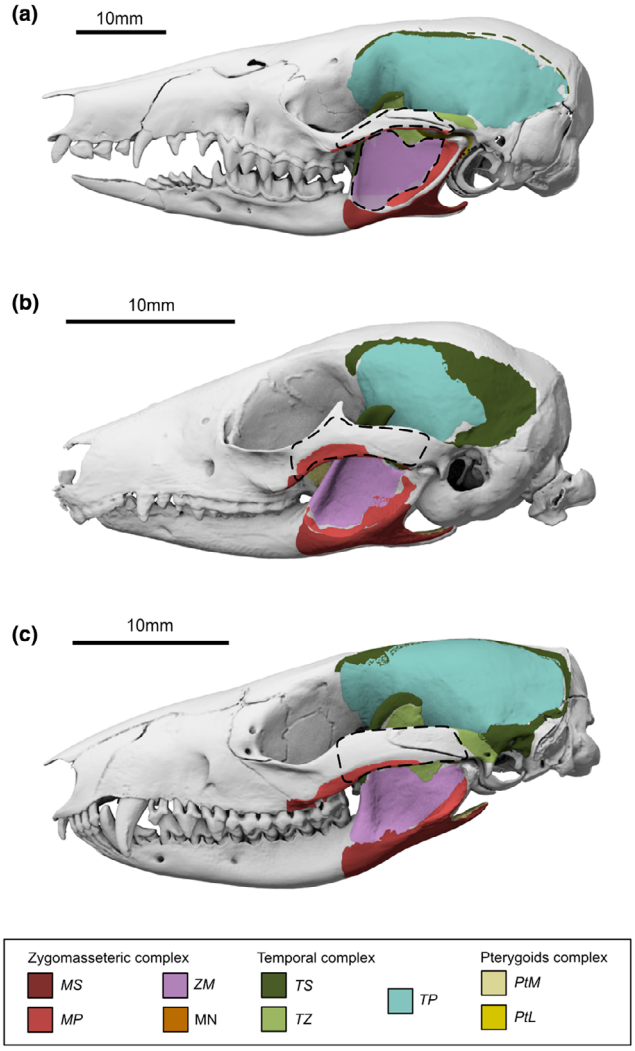

FIGURE A1 Attachment areas in *Caenolestes fuliginosus* (up), *Dromiciops gliroides* (middle) and *Monodelphis touan* (down). In dotted black line: Attachment areas of the zygomaticomandibularis (*ZM*), origins on the medial facet of the zygomatic arch. In dotted green lines: Origin of *M. temporalis pars superficialis* (TS).

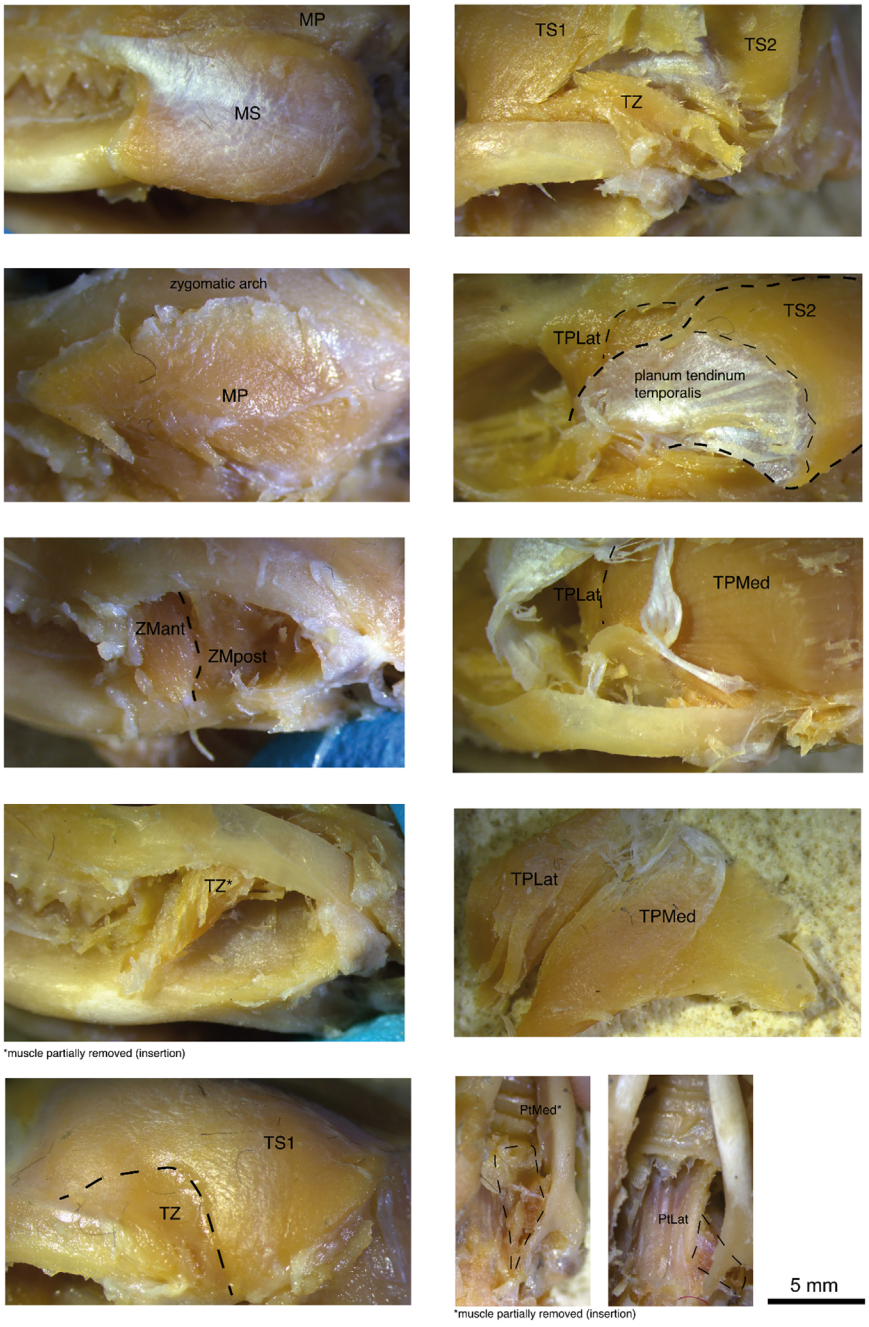

FIGURE A2 Manual dissection of *Monodelphis touan* (M2838).